Journal of Statistical Physics, Vol. 90, Nos. 1/2, 1998

An Efficient Implementation of High-Order Coupled-Cluster Techniques Applied to Quantum Magnets

Chen Zeng,[1,2] D. J. J. Farnell,[1] and R. F. Bishop[1]

Received November 14, 1996; final June 17, 1997

We illustrate how the systematic inclusion of multi-spin correlations of the quantum spin–lattice systems can be efficiently implemented within the framework of the coupled-cluster method by examining the ground-state properties of both the square-lattice and the frustrated triangular-lattice quantum antiferromagnets. The ground-state energy and the sublattice magnetization are calculated for the square-lattice and triangular-lattice Heisenberg antiferromagnets, and our best estimates give values for the sublattice magnetization which are 62% and 51% of the classical results for the square and triangular lattices, respectively. We furthermore make a conjecture as to why previous series expansion calculations have not indicated Néel-like long-range order for the triangular-lattice Heisenberg antiferromagnet. We investigate the critical behavior of the anisotropic systems by obtaining approximate values for the positions of phase transition points.

KEY WORDS: Coupled-cluster method; quantum magnets; strongly correlated spin lattices; high-order LSUB*m* approximations; generalized Néel model state; square-lattice *XXZ* model; triangular-lattice Heisenberg antiferromagnet; ket-state parametrization; bra-state parametrization; lattice animals and fundamental configurations; ground-state energy; sublattice magnetization; critical points; quantum order; quantum phase transitions.

1. INTRODUCTION

The techniques now available in the field of *ab initio* quantum many-body theory have become increasingly refined over the last decade or so. This is

[1] Department of Physics, University of Manchester Institute of Science and Technology (UMIST), P.O. Box 88, Manchester M60 1QD, United Kingdom; e-mail: R.F.Bishop@UMIST.AC.UK.

[2] Department of Physics, Syracuse University, Syracuse, New York 13210.

0022-4715/98/0100-0327$15.00/0

822/90/1-2-22

particularly true for what is nowadays recognized as one of the most powerful modern techniques, namely, the coupled-cluster method (CCM).[1–9] The results obtained from the CCM have become fully competitive with series expansions, variational calculations and quantum Monte Carlo (QMC) simulations (for the cases in which QMC may be applied).

Quantum magnets not only provide useful models of many physically realizable magnetic systems but also serve as prototypical models of quantum many-body systems. Their rich phase diagrams due to strong quantum effects have naturally provided an excellent test-bed where the above-mentioned methods can be applied and further refined. One example demonstrating rich and initially unexpected behaviour is provided by the Haldane conjecture,[10] which states that the one-dimensional (1D) spin-1 Heisenberg antiferromagnet (HAF) possesses an excitation gap, in sharp contrast to its spin-$\frac{1}{2}$ counterpart. This was surprising at the time because conventional spin-wave theory predicts a gapless excitation spectrum regardless of spin magnitude. However, the Haldane conjecture has subsequently been confirmed by numerical calculations.[11] Moreover, in the aftermath of the discovery of the superconducting cuprates, much effort has been devoted to uncovering such subtle effects as spin-nematic, spin-Peierls and chiral spin liquid orderings in two-dimensional (2D) quantum antiferromagnets, among which the frustrated quantum antiferromagnets on the triangular and the Kagomé lattices have recently attracted considerable theoretical attention.[12–21]

The CCM has been applied to various quantum magnets over the past six years. The first application of the CCM to these systems was performed by Roger and Hetherington,[22] who obtained good results at low levels of approximation for the ground-state energy of both the 1D chain and the 2D square-lattice HAF, and also for solid ^{3}He where ring exchanges of nuclear spins are considered. Since then the CCM has been applied to the isotropic (Heisenberg) and anisotropic HAF (or *XXZ* model) in 1D and on the 2D square lattice, both for spin-$\frac{1}{2}$[23–26] systems and higher-spin systems;[27, 28] to the spin-1 Heisenberg-biquadratic model;[29] and to such *frustrated* spin models as the spin-$\frac{1}{2}$ J_1-J_2 (or Majumdar-Ghosh) model[30–32] and the 2D triangular lattice HAF.[33, 34] It has also been applied to the spin-1 easy-plane ferromagnet.[35] Among these, Bishop *et al.*[23, 29] not only put forth several systematic *localised* approximation schemes to perform higher-order calculations yielding good results on the ground-state sublattice magnetizations and approximate excitation spectra, but also used an infinite-order, two-body SUB2 approximation scheme to obtain evidence of a zero-temperature quantum phase transition. For the 1D, spin-$\frac{1}{2}$ *XXZ* system it was found that the infinite-order, two-body approximation produces a value for the position of the phase transition[23]

of $\Delta = 0.3728$. This result corresponds to the exactly known antiferromagnetic phase transition point at $\Delta = 1$, and although the value obtained by the CCM is some way off the true result, it is a considerable achievement for such an *ab initio* technique to detect such a subtle (i.e., infinite order) transition at which the energy and all of its finite-order derivatives are continuous. By contrast, for the 1D, spin-1 XXZ system[29] a CCM SUB2 critical value was obtained at $\Delta = 0.7595$. Both of these values may be systematically improved considerably by the inclusion of the multi-spin correlations which are taken into account in higher-order CCM approximations discussed below.

The systematic inclusion of spin-spin correlations based on a *dimerised* state has also been made possible within the framework of the CCM,[31, 36] to study spin-Peierls ordering. This may provide a possible inroad to probe more subtle topological order in the absence of *solid* order, as in the case of the chiral spin liquid.[12, 17] The quantitative description of such phases remains one of the most challenging problems for modern microscopic quantum many-body theory in general, and the CCM in particular.

More recently, attention has been given to extending the CCM calculations to higher orders[26] in the particular case of the XXZ model, by using a *localised* approximation scheme, and by taking into account multi-spin correlations on up to 10 contiguous lattice sites in 1D and on up to 6 contiguous lattice sites in 2D. The ground-state energies, for example, are found to be in excellent agreement (i.e., within about 0.03%) with the exact result in 1D, and with those obtained from spin-wave theory,[37] series expansion analyses[38] and QMC calculations[39, 40] in 2D. However, it is fair to say that in 2D, in order to achieve the same accuracy on other more interesting physical quantities such as the ground-state sublattice magnetization and the excitation spectrum, and in order to further clarify the nature of zero-temperature quantum phase transitions, the inclusion of multi-spin correlations of still higher orders is clearly needed. Since the extent of the task of determining the CCM equations and solving them grows extremely rapidly with the approximation level, the development of efficient algorithms for performing the CCM calculations has thus become indispensable.[34]

The motivation of the present work is two-fold: (1) we wish to present a framework in which high-order CCM calculations are possible via a computational approach; and (2) we revisit the spin-$\frac{1}{2}$ quantum antiferromagnets on both the square and the triangular lattices by utilising this framework, thus allowing us to extend our previous successes in relationship to these models. We state that these results indicate that the ground-state wavefunctions of the square- and the triangular-lattice HAF both possess Néel-like long-range order, and we furthermore make a conjecture

as to why previous series expansion calculations have not indicated Néel-like long-range order for the triangular-lattice HAF.

In this article we focus on the above two models in the regimes where a Néel-like order represents the corresponding classical limit. The present method, however, should be of general utility to quantum magnets where a spin-Peierls order is relevant, for example.

A brief description of the contents of this article now follows. In Section 2 we present a general description of the CCM methodology. The ket- and bra-state formalisms are given, and the form of the ground-state energy equation, along with the characteristic CCM similarity transform, is described. The method is then applied to the square-lattice spin-$\frac{1}{2}$ XXZ antiferromagnet and the triangular-lattice spin-$\frac{1}{2}$ anisotropic antiferromagnet[15] in Sections 3 and 4 respectively. Our conclusions are given in Section 5, where we reiterate the results presented here, and also discuss briefly possibilities of further extending to even higher orders of approximation. In Appendix A, the computational method used to determine our fundamental set of configurations within a localized, LSUBm approximation scheme is described, and the derivation of the resulting CCM equations is discussed in detail.

2. THE CCM FORMALISM FOR SPIN-LATTICE MODELS

Since detailed descriptions of the fundamentals of the CCM are available in the literature,[1–9] we only highlight the essential ingredients of its application here. The exact ket and bra ground-state energy eigenvectors, $|\Psi\rangle$ and $\langle\tilde{\Psi}|$, of a many-body system described by a Hamiltonian H,

$$H|\Psi\rangle = E_g|\Psi\rangle; \qquad \langle\tilde{\Psi}|H = E_g\langle\tilde{\Psi}| \tag{1}$$

are parametrized within the single-reference CCM as follows:

$$\begin{aligned} |\Psi\rangle &= \mathrm{e}^S|\Phi\rangle; \qquad & S &= \sum_{I\neq 0} s_I C_I^+ \\ \langle\tilde{\Psi}| &= \langle\Phi|\tilde{S}\mathrm{e}^{-S}; \qquad & \tilde{S} &= 1 + \sum_{I\neq 0} \tilde{s}_I C_I^- \end{aligned} \tag{2}$$

The single model or reference state $|\Phi\rangle$ is required to have the property of being a cyclic vector with respect to two well-defined Abelian subalgebras of *multi-configurational* creation operators $\{C_I^+\}$ and their Hermitian-adjoint destruction counterparts $\{C_I^- \equiv (C_I^+)^\dagger\}$. Thus, $|\Phi\rangle$ plays the role

of a vacuum state with respect to a suitable set of (mutually commuting) many-body creation operators $\{C_I^+\}$,

$$C_I^- \,|\Phi\rangle = 0, \qquad I \neq 0 \tag{3}$$

with $C_0^- \equiv 1$, the identity operator. These operators are complete in the many-body Hilbert (or Fock) space,

$$1 = |\Phi\rangle\langle\Phi| + \sum_{I\neq 0} C_I^+ \,|\Phi\rangle\langle\Phi|\, C_I^- \tag{4}$$

Also, the *correlation operator* S is decomposed entirely in terms of these creation operators $\{C_I^+\}$, which, when acting on the model state $(\{C_I^+ \,|\Phi\rangle\})$, create excitations about the model state. We note that although the manifest Hermiticity, $(\langle\tilde{\Psi}|^\dagger = |\Psi\rangle/\langle\Psi\,|\,\Psi\rangle)$, is lost, the intermediate normalization condition $\langle\tilde{\Psi}\,|\,\Psi\rangle = \langle\Phi\,|\,\Psi\rangle = \langle\Phi\,|\,\Phi\rangle \equiv 1$ is explicitly imposed. The *correlation coefficients* $\{s_I, \tilde{s}_I\}$ are regarded as being independent variables, even though formally we have the relation,

$$\langle\Phi|\,\tilde{S} = \frac{\langle\Phi|\,\mathrm{e}^{S^\dagger}\mathrm{e}^{S}}{\langle\Phi|\,\mathrm{e}^{S^\dagger}\mathrm{e}^{S}\,|\Phi\rangle} \tag{5}$$

The full set $\{s_I, \tilde{s}_I\}$ thus provides a complete description of the ground state. For instance, an arbitrary operator A will have a ground-state expectation value given as,

$$\bar{A} \equiv \langle\tilde{\Psi}|\,A\,|\Psi\rangle = \langle\Phi|\,\tilde{S}\mathrm{e}^{-S}A\mathrm{e}^{S}\,|\Phi\rangle = \bar{A}(\{s_I, \tilde{s}_I\}) \tag{6}$$

We note that the exponentiated form of the ground-state CCM parametrization of Eq. (2) ensures the correct counting of the *independent* and excited correlated many-body clusters with respect to $|\Phi\rangle$ which are present in the exact ground state $|\Psi\rangle$. It also ensures the exact incorporation of the Goldstone linked-cluster theorem, which itself guarantees the size-extensivity of all relevant extensive physical quantities. One crucial difference between the CCM parametrization of the ground state and those used in spin-wave[37] and variational Monte Carlo calculations[41] is that although they all adopt an exponentiated form, the former (CCM) contains spin-raising operators only.

The determination of the correlation coefficients $\{s_I, \tilde{s}_I\}$ is achieved by taking appropriate projections onto the ground-state Schrödinger equations of Eq. (1). Equivalently, they may be determined variationally by requiring the ground-state energy expectation functional $\bar{H}(\{s_I, \tilde{s}_I\})$, defined as in Eq. (6), to be stationary with respect to variations in each of

the (independent) variables of the full set. We thereby easily derive the following coupled set of equations,

$$\delta\bar{H}/\delta\tilde{s}_I = 0 \Rightarrow \langle \Phi | C_I^- \, \mathrm{e}^{-S} H \mathrm{e}^S | \Phi \rangle = 0, \qquad I \neq 0 \tag{7}$$

$$\delta\bar{H}/\delta s_I = 0 \Rightarrow \langle \Phi | \tilde{S} \mathrm{e}^{-S} [H, C_I^+] \, \mathrm{e}^S | \Phi \rangle = 0, \qquad I \neq 0 \tag{8}$$

Equation (7) also shows that the ground-state energy at the stationary point has the simple form

$$E_g = E_g(\{s_I\}) = \langle \Phi | \, \mathrm{e}^{-S} H \mathrm{e}^S | \Phi \rangle \tag{9}$$

It is important to realize that this (bi-)variational formulation does *not* lead to an upper bound for E_g when the summations for S and $\tilde{S}$ in Eq. (2) are truncated, due to the lack of exact Hermiticity when such approximations are made. However, it is clear that the important Hellmann–Feynman theorem *is* preserved in all such approximations.

We also note that Eq. (7) represents a coupled set of nonlinear polynomial equations for the c-number correlation coefficients $\{s_I\}$. The nested commutator expansion of the similarity-transformed Hamiltonian,

$$\hat{H} \equiv \mathrm{e}^{-S} H \mathrm{e}^S = H + [H, S] + \frac{1}{2!} [[H, S], S] + \cdots \tag{10}$$

together with the fact that all of the individual components of S in the sum in Eq. (2) commute with one another, imply that each element of S in Eq. (2) is linked directly to the Hamiltonian in each of the terms in Eq. (10). Thus, each of the coupled equations (7) is of linked cluster type. Furthermore, each of these equations is of finite length when expanded, since the otherwise infinite series of Eq. (10) will always terminate at a finite order, provided (as is usually the case) that each term in the second-quantised form of the Hamiltonian H contains a finite number of single-body destruction operators, defined with respect to the reference (vacuum) state $|\Phi\rangle$. Therefore, the CCM parametrization naturally leads to a workable scheme which can be efficiently implemented computationally. It is also important to note that at the heart of the CCM lies a similarity transformation, in contrast with the unitary transformation in a standard variational formulation in which the bra state $\langle \tilde{\Psi} |$ is simply taken as the explicit Hermitian adjoint of $|\Psi\rangle$.

In the following sections we describe CCM results for anisotropic Heisenberg antiferromagnets on both the square and triangular lattices, and the reader should note that these results were obtained using a new computational approach which is described in Appendix A.

3. SPIN-$\frac{1}{2}$ *XXZ* ANTIFERROMAGNET ON THE 2D SQUARE LATTICE

In this section we shall consider the spin-$\frac{1}{2}$ XXZ model on the infinite square lattice. The XXZ Hamiltonian is given by,

$$H = \sum_{\langle i, j \rangle} [s_i^x s_j^x + s_i^y s_j^y + \Delta s_i^z s_j^z] \tag{11}$$

where the sum on $\langle i, j \rangle$ runs over all nearest-neighbour pairs and counts each pair only once. The square-lattice XXZ model has no exact solution, unlike its 1D counterpart, although approximate analytical and numerical calculations have been performed. To put later CCM calculations in context, we note that the XXZ model has three regimes: an Ising-like phase characterized by non-zero Néel order; a planar-like phase in which the spins in the ground-state wavefunction are believed to lie in the xy plane; and a ferromagnetic phase. A Monte Carlo study of the 2D anisotropic Heisenberg model was performed by Barnes *et al.*[43] They observed that the staggered magnetization in the z-direction is non-zero for $\Delta > 1$, but then appears to become zero below $\Delta = 1$. They therefore conclude that the critical point is probably very near to this point. In contrast to this Monte Carlo calculation, Kubo and Kishi[44] have used sum rules to investigate the ground state of this system. They state that the ground state possesses an off-diagonal long-range order (LRO) akin to that of the XY-like state at small anisotropy, $0.0 < \Delta < 0.13$. Also, for $\Delta > 1.78$ they observe that the system demonstrates non-zero Ising-like LRO. At $\Delta = -1$ there is a first-order phase transition to the ferromagnetic phase for this model.

The isotropic Heisenberg point has been extensively studied using various approximate methods, and so shall be used as a test case for the CCM results discussed later in this section. Runge[40] has performed the most accurate Monte Carlo simulation to date for the square-lattice, isotropic HAF. This provides a value for the ground-state energy per spin of $-0.66934(4)$, and a value for the sublattice magnetization which is $61.5\% \pm 0.5\%$ of the classical value. In comparison, linear spin-wave theory (LSWT)[37] gives a value of -0.658 for the ground-state energy, and a value for the sublattice magnetization which is 60.6% of the classical value.

A. The Model State

We begin the CCM treatment of this spin system by choosing a suitable model state $|\Phi\rangle$ (for a particular regime), such that all other

possible spin configurations may be obtained by the application of linear combinations of products of spin-raising operators to this state. In the Ising-like regime, characterized by non-zero Néel order, a natural choice for the model state is the Néel state with spins lying along the z axis. (For clarity, this state will be referred to as the z-axis Néel model state throughout this article.) We note however that this model state is not the best choice for all values of Δ because the ground-state wavefunction of the XXZ model in the region $-1 < \Delta < 1$ is believed to contain only spins which lie in the xy plane. In this regime, we again use the classical Néel state, but this time with spins lying on the x axis. (This state will be referred to as the planar model state throughout this article.) Hence, we see that even for the same spin model and lattice a different choice of model state may be preferable, depending on the regime that we are investigating.

We shall consider the Ising-like regime first, and, so that spins on either sublattice may be treated equivalently, we peform a rotation of the local axes of the up-pointing spins by 180° about the y axis. The transformation is described by,

$$s^x \to -s^x, \qquad s^y \to s^y, \qquad s^z \to -s^z \tag{12}$$

The model state now appears *mathematically* to consist of purely down-pointing spins which is precisely given by Eq. (A1) of Appendix A. In terms of the spin raising and lowering operators $s_k^{\pm} \equiv s_k^x \pm i s_k^y$ the Hamiltonian may be written in these local axes as,

$$H = -\frac{1}{2} \sum_{\langle i, j \rangle}^{N} [s_i^+ s_j^+ + s_i^- s_j^- + 2\,\Delta s_i^z s_j^z] \tag{13}$$

For the planar model state, we again rotate the local axes of these spins on the separate sublattices such that all spins appear to be lie along the negative z direction which is again given by Eq. (A1). This is achieved by rotating the axes of the left-pointing spins (i.e., those pointing along the negative x direction) in the planar model state by 90° about the y axis, and by rotating the axes of the right-pointing spins (i.e., those pointing along the positive x direction) by 270° about the y axis. (The positive z-axis is defined to point directly upwards, and the positive x-axis is defined to point directly to the right.) Hence the transformation of the local axes of the left-pointing spins is described by,

$$s^x \to s^z, \qquad s^y \to s^y, \qquad s^z \to -s^x \tag{14}$$

and the transformation of the local axes of the right-pointing spins is described by,

$$s^x \to -s^z, \qquad s^y \to s^y, \qquad s^z \to s^x \tag{15}$$

The transformed Hamiltonian for the planar model state is now given by,

$$H = -\frac{1}{4} \sum_{\langle i,j \rangle}^{N} [(\Delta + 1)(s_i^+ s_j^+ + s_i^- s_j^-) + (\Delta - 1)(s_i^+ s_j^- + s_i^- s_j^+) + 4 s_i^z s_j^z] \tag{16}$$

In the remainder of this section, the power and flexibility of our new formalism is illustrated by focussing primarily on the planar model state applied to the XXZ model on the square lattice. Note however that equivalent calculations have been undertaken for the z-axis Néel model state, and that a general explanation is presented here only. A more detailed explanation of CCM calculations that deal with both the ground-state properties and the excitation spectrum using the new formalism for the XXZ model based on this model state will be presented in ref. 42.

B. Fundamental Excitation Configurations: Lattice Animals

The "localised" LSUBm approximation scheme defined in Appendix A is used in this section, and the first step of our modular solution is therefore to obtain the set of fundamental configurations for a given approximation scheme by utilising appropriate lattice symmetries. Another constructive way to define the LSUBm scheme used here for the square lattice is to consider a right-angled *bounding triangle* containing m lattice points along the sides parallel to the axes (see Fig. 1 for a diagram of this construction where the bounding triangle for LSUB4 is shown). All possible fundamental configurations for the LSUBm approximation are then confined by this bounding triangle. This comes about because it is easy to show that all connected configurations of size m (or the lattice animals of size m) are constrained to lie within or on this bounding triangle. Furthermore, as first shown by Lunnon,[45] the introduction of this bounding triangle greatly simplifies the recursive procedure of *growing* a connected cluster of given size. The disconnected configurations for the LSUBm scheme are then constructed by successively considering all "subsets" of each member of the fundamental set of connected configurations, and all possible disconnected configurations are thereby generated. (The "subsets" here refer to all independent configurations which are formed by removing one or more spins from these connected configurations.)

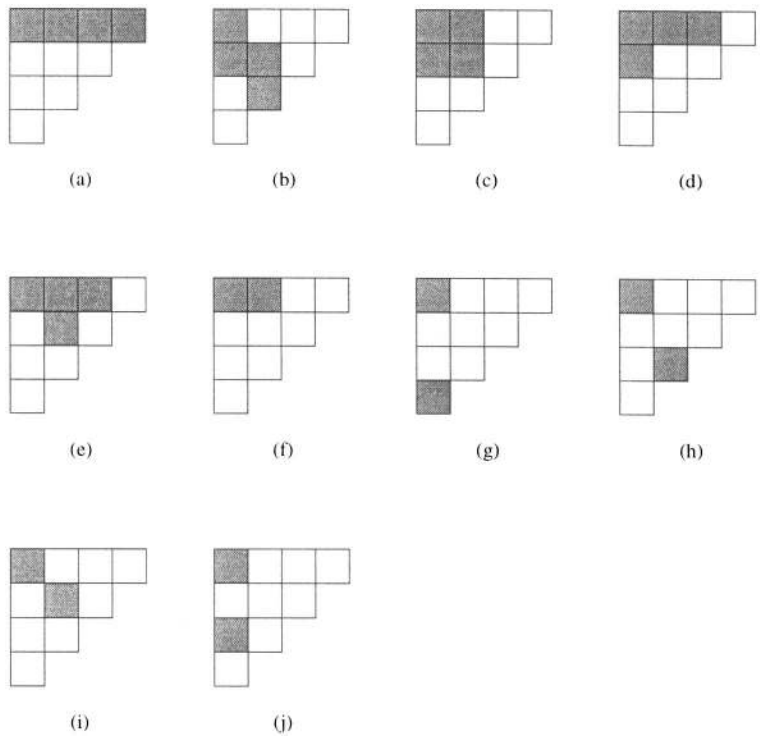

Fig. 1. The square lattice LSUB4 bounding triangle is shown in this figure along with the LSUB4 lattice animals, illustrated by diagrams (a)–(c). The fundamental LSUB4 configurations for the planar model state are given by diagrams (a)–(j), and the fundamental configurations for the z-axis Néel model state form a subset of them, namely, all diagrams except (c), (i), and (j). The centres of the shaded squares mark the relative positions of the sites of the square lattice on which the spins are flipped with respect to the model state.

To be specific, for the square lattice, there are four rotational operations, (0°, 90°, 180°, 270°), and four reflections, (along the x and y axes, and along the lines $x = y$ and $x = -y$), which preserve the symmetries of both the lattice and the Hamiltonian. Moreover, the Hamiltonian of Eq. (16), which is defined with respect to the planar model state, contains only even products of spin-flip operators and a single term containing two s^z operators. Repeated application of this Hamiltonian to this model state yields the ground state (assuming that this model state is not orthogonal to it). Therefore the ground state will have an even numbers of spin flips with respect to this model state, and so we restrict the LSUBm approximations to contain even numbers of spin-raising operators in the ket-state

correlation operator, S, only for this planar model state. As an example, in Fig. 1 we show all 10 fundamental configurations retained in the LSUB4 approximation when the planar model state is used in the CCM calculation.

Further reduction in the number of fundamental configurations can be made when the z-axis Néel model state is used in the CCM calculations. This comes about because, although the total uniform magnetisation $s_T^z = \sum_i s_i^z$ (where s_i^z is defined with respect to a global quantisation axis and the sum on the index i runs over all lattice sites) is always a good quantum number independent of the model state used, only the z-axis Néel model state is an eigenstate of the total uniform magnetisation s_T^z. In contrast, the planar model state is not an eigenstate of the total uniform magnetization s_T^z. Therefore, for the z-axis model state case one can explicitly conserve s_T^z by restricting the fundamental configurations to those which produce no change in s_T^z with respect to the z-axis Néel model state. This restriction, for example, reduces the number of the fundamental configurations retained in the LSUB4 approximation to 7 if the z-axis Néel model state is employed in the CCM calculations, and see Fig. 1. We tabulate the number of of fundamental configurations up to the LSUB8 level of approximation for both model states in Table I. Note that only the CCM calculations based on the z-axis Néel model state are actually carried out up to LSUB8 approximation in this article.

Table I. Results Obtained for the Spin-1/2 *XXZ* Model on the 2D Square Lattice Using CCM LSUB*m* Approximations ($m = 2, 4, 6, 8$)[a]

m	N_{F_1}	N_{F_2}	E_g/N ($\Delta = 1$)	M^+ ($\Delta = 1$)	Δ_{c_1}	Δ_{c_2}	Δ_{c_3}
2	1 (1 + 0)	1 (1 + 0)	−0.64833	0.8414	—	—	—
4	10 (6 + 4)	7 (5 + 2)	−0.66366	0.7648	−1.249	1.648	0.577
6	131 (41 + 90)	75 (29 + 46)	−0.66700	0.7273	−1.083	1.286	0.7631
8	2793 (410 + 2383)	1287 (259 + 1028)	−0.66817	0.7048	?	?	0.8429
∞	—	—	−0.66968	0.62	—	—	—

[a] Here N_{F_1} denotes the number of fundamental configurations for the planar model state, which are further decomposed in terms of connected and disconnected ones respectively, and N_{F_2} denotes the number of fundamental configurations for the z-axis Néel model state. The ground-state energy per spin, E_g/N, and the sublattice magnetization, M^+, at the isotropic Heisenberg point ($\Delta = 1$) are shown, as well as extrapolated results in the limit $m \to \infty$. Various critical anisotropy parameters are also given. Δ_{c_1} and Δ_{c_2} indicate the LSUB*m* critical points for the planar model state corresponding to the ferromagnetic and antiferromagnetic phase transitions. Δ_{c_3} indicates the critical point for the z-axis Néel model state corresponding to the antiferromagnetic phase transition. Note that there are no terminating points in the LSUB2 approximation.

C. Similarity-transformed Hamiltonian and CCM Ket-State Equations

In order to solve the Schrödinger equation of Eq. (1), we shall specifically utilise the Hamiltonian of Eq. (16), although a comparable analysis can also be performed for Eq. (13). The expression for the ket-state correlation operator of Eq. (A2) is now used to write the similarity-transformed Hamiltonian, $\hat{H}$, of Eq. (10) in terms of the operators F_k and G_{km}. Furthermore, we subdivide $\hat{H}$ into three categories as discussed in Appendix A to clarify the problem of finding the CCM equations, where $\hat{H}\,|\Phi\rangle \equiv e^{-S}He^{S}\,|\Phi\rangle = (\hat{H}_1 + \hat{H}_2 + \hat{H}_3)\,|\Phi\rangle$, such that:

$$\hat{H}_1 = \frac{1}{2}\sum_{k\rho}\left\{-(G_{km} + F_k F_m) + \frac{1}{4}(\Delta - 1)(F_m^2 + F_k^2)\right\} s_k^+ s_m^+$$

$$-\frac{1}{8}(\Delta + 1)\sum_{k\rho}\{1 + 2G_{km}^2 + 4G_{km}F_kF_m + F_k^2F_m^2\}\, s_k^+ s_m^+ \tag{17}$$

$$\hat{H}_2 = \frac{1}{4}\sum_{k\rho}\left\{F_m s_m^+ + F_k s_k^+ + \frac{1}{2}(1 - \Delta)(F_m s_k^+ + F_k s_m^+)\right\}$$

$$+\frac{1}{8}(\Delta + 1)\sum_{k\rho}\{(2G_{km} + F_kF_m)(F_m s_m^+ + F_k s_k^+)\} \tag{18}$$

$$\hat{H}_3 = -\frac{1}{8}\sum_{k\rho}\{1 + (\Delta + 1)(G_{km} + F_kF_m)\} \tag{19}$$

Note that k runs over all lattice sites and that m is given by $m \equiv k + \rho$, such that ρ covers all nearest neighbours to k. Hence we see from Eq. (19) that the ground-state energy of the XXZ model for the planar model state is given by,

$$\frac{E_g}{N} = -\frac{z}{8}[2x_1(\Delta + 1) + 1] \tag{20}$$

where $x_1 \equiv [k, k + \rho]$ (see Appendix A) represents all nearest-neighbour, two-body correlation coefficients in Eq. (A2) which are equivalent under the translational and rotational symmetries of the lattice, and z represents the lattice coordination number (i.e., the number of nearest neighbours to a given site), namely $z = 4$ for the square lattice considered here. Note that the ground-state energy of Eq. (20) is *exact* in the sense that both the exact

expansion for S and any non-trivial approximation of it will always produce this expression.

D. Results

1. Ground-State Energy. The ground-state energy for the planar model state is illustrated by Fig. 2, and we can see that these results appear to be in good agreement with Monte Carlo results.[43] The highest approximation that has been attempted for the planar model state is the LSUB6 approximation, which contains 131 fundamental configurations and gives a ground-state energy per spin of -0.66700 at the Heisenberg point. For the z-axis Néel model state, due to the reduced number of fundamental configurations, we were able to solve the LSUB8 approximation, which contains 1287 fundamental configurations and gives an energy per spin of -0.66817 at $\Delta = 1$. Hence, by utilising the new formalism we have increased the number of fundamental configurations used in a CCM calculation for the z-axis Néel model state by over an order of magnitude compared to the previous best (i.e., LSUB6[27] which contains 75 configurations). Table I summarises the information regarding numbers of configurations and ground-state energies at $\Delta = 1$. Note that the calculations for both model states at the Heisenberg point give exactly the same results at equivalent approximation levels, and so only one figure for the

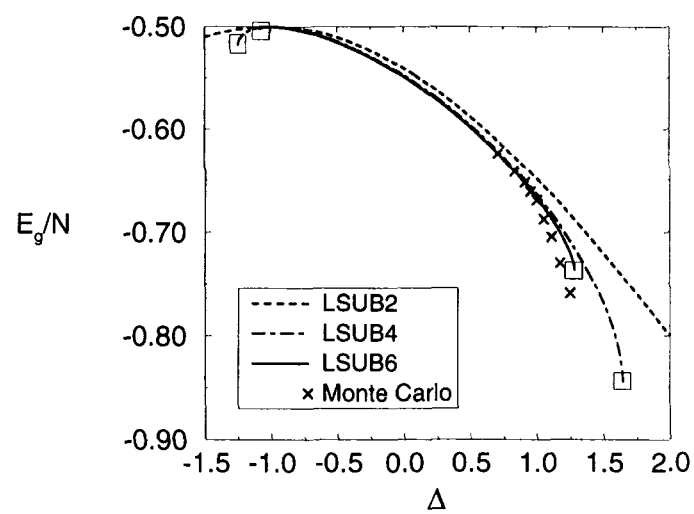

Fig. 2. Results for the CCM ground-state energy of the XXZ model on the 2D square lattice using the planar model state, compared to the Monte Carlo results of ref. 44. LSUBm critical points Δ_{c_1} and Δ_{c_2} are indicated by the boxes.

ground-state energy is quoted in Table I. The reason for the equivalence is that the Hamiltonians of Eqs. (13) and (16) become identical at $\Delta = 1$. Also, all of the correlation coefficients for configurations at a given LSUBm level contained in the planar model state case but not contained in the z-axis Néel model state case become identically zero at $\Delta = 1$.

In order to compare our results to other approximate calculations, described at the beginning of Sec. 3, we perform a "naive" extrapolation of our LSUBm ground-state energies at the isotropic Heisenberg point. Note that we shall not seek to justify this particular form for the extrapolation in this article, but we simply note that it has been found useful previously[26] and that it will be discussed more fully elsewhere.[42] As in ref. 26 we plot these energies against $1/m^2$ and extrapolate these in the limit $m \to \infty$. We obtain an extrapolated value for the ground-state energy of -0.66968 which compares favourably to the result of Runge[40] of $-0.66934(4)$.

The results for the z-axis Néel model state are found to be less accurate than those using the planar model state in the region $-1 < \Delta < 1$. Conversely, for $\Delta > 1$, the results based on the z-axis Néel model state become the more accurate of the two sets of calculations. This therefore vindicates our decision to use two separate model states in order to investigate the Ising- and planar-like phases of this model.

Beyond certain values of the anisotropy parameter (called critical points) it is found that there is no physically reasonable solution to the LSUBm CCM equations for $m \geqslant 4$. This characteristic breakdown of the solution to the CCM equations has previously been related to a phase transition of the real system.[27] We also note that the second derivative of the ground-state energy may be obtained analytically and it is found that this quantity diverges at the LSUBm critical points. Table I illustrates two sets of estimates for the critical points for the XXZ model based on the planar model state, Δ_{c_1} and Δ_{c_2}, corresponding to the ferromagnetic and antiferromagnetic phase transition points respectively. Encouragingly, the critical points Δ_{c_1} corresponding to the ferromagnetic phase transition become closer to $\Delta = -1$ with increasingly refined approximation level. Table I also includes the estimates Δ_{c_3} for the critical points obtained for the z-axis Néel model state corresponding to the antiferromagnetic phase transition point. Note that LSUBm results based on these two model states always bound the Heisenberg point, at which the true antiferromagnetic phase transition is believed to lie, and also appear to converge with increasing m.

2. Sublattice Magnetization. We now consider a simple order parameter called the sublattice magnetization, $M^+ \equiv -2\langle s^z \rangle$, which is defined in terms of the local, rotated spin axes. Hence M^+ is given by,

$$M^+ = \frac{-2}{N_0} \sum_{i=1}^{N_0} \langle \tilde{\Psi} | s_i^z | \Psi \rangle = 1 - \frac{2}{N_0} \sum_{k=1}^{N_0} \langle \Phi | \tilde{S} F_k s_k^+ | \Phi \rangle$$

$$= 1 - 2 \sum_{r=1}^{N_F} n_r (n_r!) \, \tilde{x}_r x_r \tag{21}$$

where the index i runs over all N_0 sites of a sublattice, and N_F again indicates the total number of configurations for a given LSUBm approximation level. Note that $\tilde{x}_r$ and x_r, respectively, are bra- and ket-state correlation coefficients associated with the rth fundamental configuration, described in Appendix A, and that n_r is the number of spins in this configuration. From Eq. (21) we can see that in order to obtain a numerical value for the sublattice magnetization we must first know the values of both the ket- and bra-state correlation coefficients. The manner in which we determine these coefficients is described in Appendix A. Our results for the XXZ model using the planar model state are shown in Fig. 3, and we note that these results appear to converge to a non-zero value as one increases the approximation level. Hence our results indicate non-zero Néel-type long-range order in the xy plane for the square lattice in the planar regime. Table I also summarises the results for the sublattice magnetization at the Heisenberg point. Note that results based on both

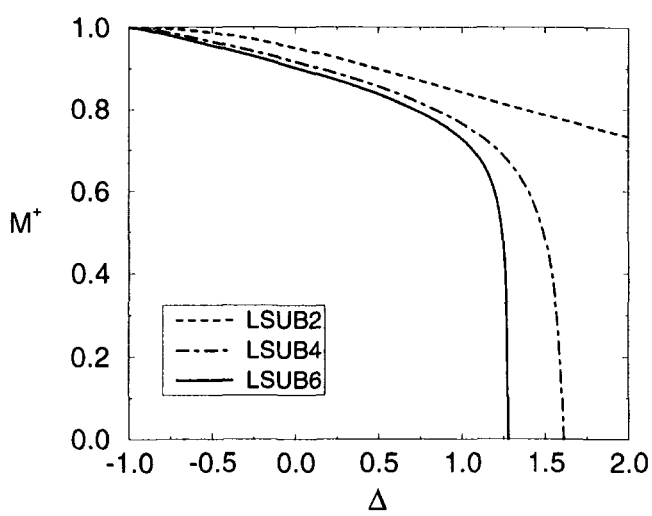

Fig. 3. Results for the CCM sublattice magnetization of the XXZ model on the 2D square lattice using the planar model state. CCM results indicate non-zero, in-plane long-range order in the region $-1 < \Delta < 1$.

model states are again found to be identical at this point and so only a single number is quoted in Table I.

Again, in order to compare our results to other approximate calculations, we perform a "naive" extrapolation of our LSUBm sublattice magnetizations at the isotropic Heisenberg point. We plot the LSUBm sublattice magnetization against $1/m$ and extrapolate these in the limit $m \to \infty$. This particular choice of extrapolation has been found useful previously,[26] and will be discussed more fully elsewhere.[42] We obtain an extrapolated value for the sublattice magnetization of 0.62 which again compares very favourably to the result of Runge[40] of 0.615.

In summary, the new CCM formalism has been used in order to calculate estimates of the ground-state energy and sublattice magnetization for the 2D XXZ model, and these results are found to be in good agreement with other approximate calculations. The highest-order approximation for the z-axis Néel model state has been extended to LSUB8 level using the new formalism, which is an increase of over an order of magnitude in the number of fundamental configurations used in the previous-highest LSUB6 calculation. Also, the positions of the phase transition points obtained by the CCM, using both model states, are fully consistent with the known behaviour for this model. Finally, the results presented here also support the idea that this model contains both Ising- and planar-like phases.

4. SPIN-$\frac{1}{2}$ TRIANGULAR-LATTICE ANTIFERROMAGNET

Unlike the square-lattice spin-$\frac{1}{2}$ HAF where various calculations including extensive quantum QMC simulations[39, 40] strongly support the existence of a Néel ordering with a reduced magnetic moment of about 62% of its classical value (See Sec. 3), the three-sublattice ordering for the corresponding triangular case is much less clear. For instance, early variational wavefunction calculations[41] that include long-ranged two-spin and nearest-neighbour three-spin correlations support an ordered ground state with a value of the sublattice magnetization, $M^+ = 0.68$, i.e., as large as 68% of the classical value. Based on this antiferromagnetic correlated trial wavefunction, fixed-node Green function Monte Carlo (GFMC) simulations were recently performed on lattices of up to 324 sites.[46] These yielded a similar magnetization, $M^+ \approx 0.60$.[46] However, series expansion calculations,[15] utilising up to 11th-order terms in an Ising-like anisotropy parameter suggest that the triangular HAF may be at, or at least close to (with the magnetisation being extrapolated to a value of $M^+ \approx 0.20$), the critical point of losing magnetic order. This scenario has received support from exact diagonalisation calculations on lattices of up to 36 sites.[47] Yet another careful analysis[20] of the same data from exact diagonalisations in

terms of a consistent description of the symmetries and dynamics of the quasi-degenerate joint states indicates the presence of sublattice magnetic order with the magnetization value, $M^+ \approx 0.50$, which is also consistent with second-order spin-wave calculations.[21] Clearly, further work is still needed to account for the discrepancy, and to provide a more definite and converged result.

Hence, in this section we therefore further apply the CCM to the spin-$\frac{1}{2}$ triangular HAF and focus on model-specific details of the algorithm implementation discussed in Sec. 2. Compared with earlier applications of the CCM on the triangular HAF which only include two-spin (though long-ranged) correlations,[33] the current calculations, which take into account all multi-spin correlations on up to six contiguous sites, have obtained various ground-state properties that are now found to be fully competitive with those obtained from the above-mentioned methods.

A. Model Hamiltonian and Model State

The spin-$\frac{1}{2}$ triangular HAF is described by the antiferromagnetic-coupling Hamiltonian,

$$H = \sum_{\langle i, j \rangle} \vec{s}_i \cdot \vec{s}_j \tag{22}$$

where $\vec{s}_i$ denotes the spin-$\frac{1}{2}$ operator at site i on the infinite triangular lattice. The sum in Eq. (22) on $\langle i, j \rangle$ runs over all nearest-neighbour pairs and counts each pair once. We note that the operators in Eq. (22) are defined in terms of some global spin quantisation axes referring to all spins, whereas henceforth we shall consistently employ a notation in which the spin operators are described in terms of local (Néel-like) quantisation axes for each of the three sublattices (A, B, and C) of the triangular lattice. The classical ground state of Eq. (22) is the Néel-like state where all spins on each sublattice are separately aligned (all in the xz-plane, say). The spins on sublattice A are oriented along the negative z-axis, and spins on sublattices B and C are oriented at $+120°$ and $-120°$, respectively, with respect to the spins on sublattice A. In order both to facilitate the extension of the isotropic Heisenberg antiferromagnet to include an Ising-like anisotropy first introduced by Singh and Huse[15] and to make a suitable choice of the CCM model state, we perform the following spin-rotation transformations. Specifically, we leave the spin axes on sublattice A unchanged, and we rotate about the y-axis the spin axes on sublattices B and C by $-120°$ and $+120°$ respectively,

$$
\begin{aligned}
&s_B^x \to -\frac{1}{2}s_B^x - \frac{\sqrt{3}}{2}s_B^z; \qquad && s_C^x \to -\frac{1}{2}s_C^x + \frac{\sqrt{3}}{2}s_C^z \\
&s_B^y \to s_B^y; && s_C^y \to s_C^y \\
&s_B^z \to \frac{\sqrt{3}}{2}s_B^x - \frac{1}{2}s_B^z; && s_C^z \to -\frac{\sqrt{3}}{2}s_C^x - \frac{1}{2}s_C^z
\end{aligned}
\tag{23}
$$

We may rewrite Eq. (22) in terms of spins defined in these local quantisation axes for the triangular lattice with a further introduction of an anisotropy parameter λ for the non-Ising-like pieces,

$$
\begin{aligned}
H = \sum_{\langle i \to j \rangle} \Big\{ & -\frac{1}{2}s_i^z s_j^z + \frac{\sqrt{3}\,\lambda}{4}(s_i^z s_j^+ + s_i^z s_j^- - s_i^+ s_j^z - s_i^- s_j^z) \\
& + \frac{\lambda}{8}(s_i^+ s_j^- + s_i^- s_j^+) - \frac{3\lambda}{8}(s_i^+ s_j^+ + s_i^- s_j^-) \Big\}
\end{aligned}
\tag{24}
$$

where $\lambda = 1$ corresponds to the isotropic Heisenberg Hamiltonian of Eq. (22). We note that the summation in Eq. (24) again runs over nearest-neighbour bonds, but now also with a *directionality* indicated by $\langle i \to j \rangle$, which goes from A to B, B to C, and C to A. When $\lambda = 0$, the Hamiltonian in Eq. (24) describes the usual classical Ising system with a unique ground-state which is simply the fully aligned ("ferromagnetic") configuration in the local spin coordinates described above. We choose this state as the uncorrelated CCM model state $|\Phi\rangle$ which is, of course, precisely given by Eq. (A1) of Appendix A.

B. Fundamental Excitation Configurations: Lattice Animals

Unlike the square lattice case discussed in Sec. 3B where all lattice point-group symmetries are employed to produce symmetry-distinct configurations, care must be exercised here since not all of the lattice point-group symmetries leave the lattice-spin Hamiltonian invariant. The Hamiltonian of Eq. (24) (or the CCM model state) explicitly breaks some of the lattice symmetries because of the presence of bond-directionality in the Hamiltonian. Thus only 6 (instead of the full 12) point-group symmetries should be used in the symmetry reduction. These are, specifically, three rotational operations (0°, 120°, and 240°) together with three reflections about the lattice axes (i.e., lines that coincide with the edges of the triangular lattice). For example, the three configurations (a), (b), and (c) shown in Fig. 4 are symmetry equivalent, as are the three configurations

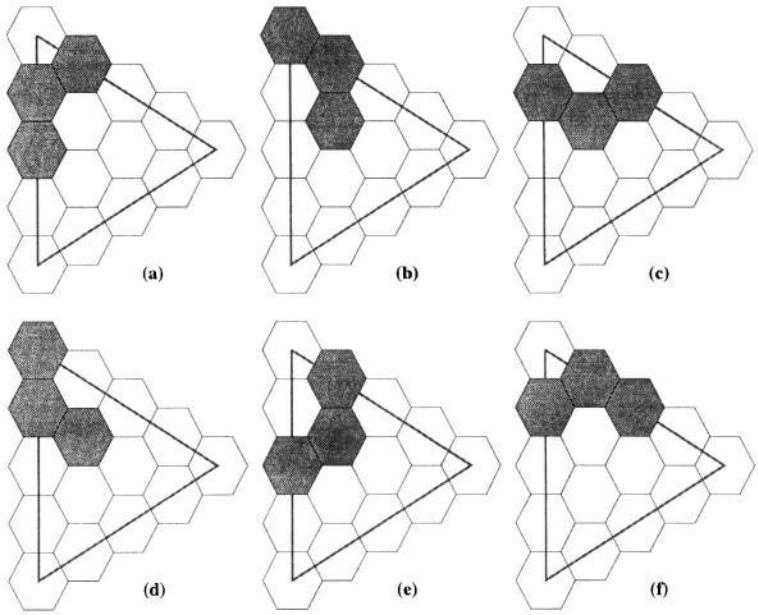

Fig. 4. The LSUB5 bounding triangle and symmetry-related correlation configurations for the triangular lattice. The centres of the shaded hexagons mark the relative position of the sites of the triangular lattice on which the spins are flipped with respect to the model state. See text for details.

(d), (e), and (f). However, the former are regarded as inequivalent to the latter in the context of the present spin-lattice Hamiltonian problem. For the purpose of comparison with the case in, say, percolation problems, and for the sake of concreteness, let us consider the connected configurations of size 6. If all 12 point-group symmetries were used, we would have obtained 82 symmetry-inequivalent configurations as shown in Fig. 5, which are further classified into two groups: 17 in group group A and 65 in group B. The configurations in group A are of higher symmetries than those in group B, and thus do not lead to new symmetry-inequivalent configurations when only 6 point-group symmetries must be used in the symmetry reduction as discussed above. Each configuration in group B, however, results in another new symmetry-inequivalent configuration. Therefore, the total number of symmetry-inequivalent connected configurations of size 6 is 147 for the present spin-Hamiltonian problem. The set of symmetry-inequivalent configurations (connected and disconnected) thereby forms the set of fundamental configurations. We tabulate the number of fundamental configurations up to the LSUB7 level of approximation in

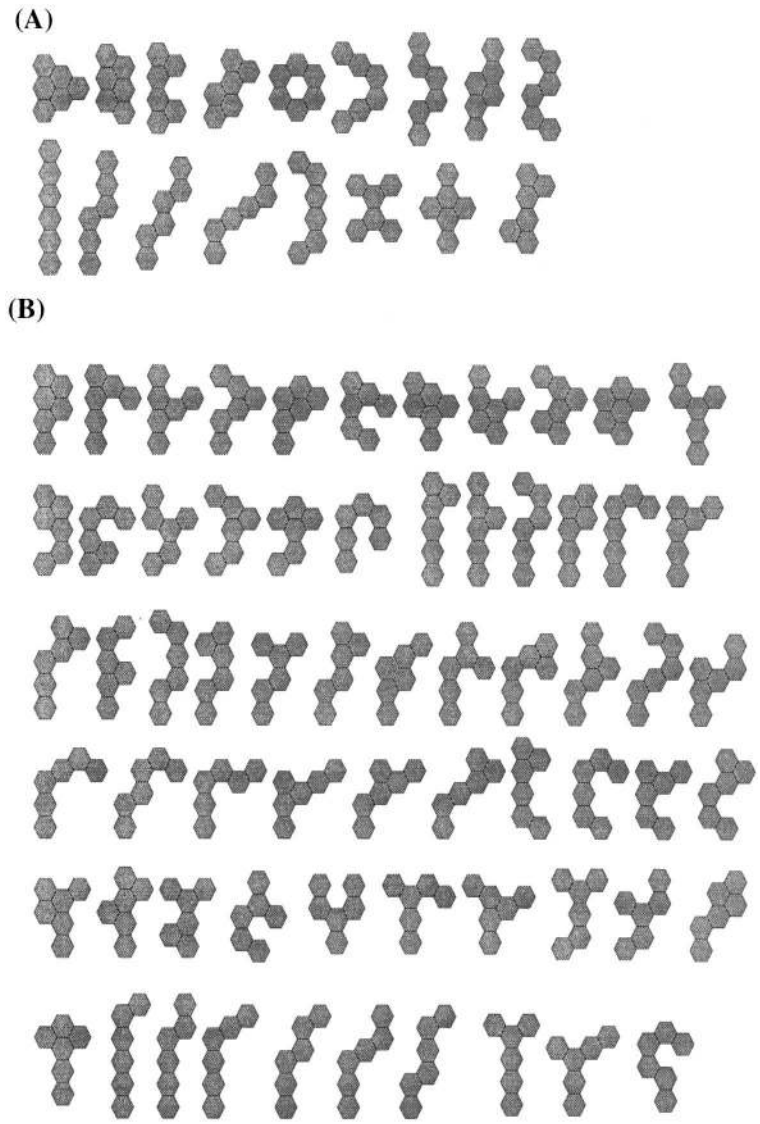

Fig. 5. All 82 lattice animals of size 6 on a triangular lattice after symmetry reduction including translational and 12 point-group symmetry operations (see text for details). The centres of the hexagons mark the relative position of the sites of the triangular lattice on which the spins are flipped with respect to the model state. See text for a discussion of group A and group B diagrams.

Table II. Results Obtained for the Spin-1/2 Triangular-Lattice HAF Using CCM LSUBm Approximations ($m = 2, 3, 4, 5, 6, 7$)[a]

m	N_F	E_g/N ($\lambda = 1$)	M^+ ($\lambda = 1$)	λ_{c_1}	L_{c_2}
2	2 (2 + 0)	−0.50290	0.8578		
3	8 (6 + 2)	−0.51911	0.8045	−0.86	5.47
4	30 (16 + 24)	−0.53427	0.7273	−0.65	2.20
5	143 (53 + 90)	−0.53869	0.6958	−0.60	1.98
6	758 (200 + 558)	−0.54290	0.6561	−0.55	1.77
7	4427 (837 + 3590)	?	?	?	?
∞	—	−0.5505	0.51		

[a] Here N_F denotes the number of fundamental configurations which are further decomposed in terms of connected and disconnected ones respectively. Note that only CCM calculations up to the LSUB6 level of approximations are performed in this article. The ground-state energy per spin, E_g/N, and the sublattice magnetization, M^+, at the isotropic Heisenberg point ($\lambda = 1$) are shown for each LSUBm approximation, as well as extrapolated results in the limit $m \to \infty$. The terminating anisotropy parameters, λ_{c_1} and λ_{c_2}, which correspond respectively to a phase transition at $\lambda = -\frac{1}{2}$ and another believed[15] to be near $\lambda = 1$, are also given for each LSUBm approximation. Note that there is no terminating point in the LSUB2 approximation.

Table II. Note that only CCM computations up to the LSUB6 level of approximation are actually carried out in this article.

C. Similarity-Transformed Hamiltonian and CCM Ket-State Equations

Using Eq. (A5) given in Appendix A, we can straightforwardly carry out the similarity transformation of the Hamiltonian given by Eq. (24); the resulting terms are further classified into three categories for reasons discussed in Appendix A, i.e., $\hat{H}\,|\Phi\rangle \equiv e^{-S} H e^{S}\,|\Phi\rangle = (\hat{H}_1 + \hat{H}_2 + \hat{H}_3)\,|\Phi\rangle$, as indicated below:

$$\begin{aligned}\hat{H}_1 = \frac{1}{4}\sum_{k\rho}\Big\{ & -2(G_{km} + F_k F_m) \\ & -\frac{3\lambda}{2} + \sqrt{3}\,\lambda(F_k - F_m)(1 + 2G_{km} + F_k F_m)\Big\}\, s_k^+ s_m^+ \\ & + \frac{1}{4}\sum_{k\rho}\Big\{ -\frac{\lambda}{2}(F_m^2 + F_k^2) - 3\lambda G_{km}^2 - 6\lambda G_{km} F_k F_m - \frac{3\lambda}{2} F_k^2 F_m^2 \Big\}\, s_k^+ s_m^+ \end{aligned} \tag{25}$$

$$\hat{H}_2 = \frac{1}{4}\sum_{k\rho}\left\{\left[F_m - \frac{\sqrt{3}\,\lambda}{2}(1-F_m^2) + \frac{\lambda}{2}F_k\right]s_m^+ + \left[F_k + \frac{\sqrt{3}\,\lambda}{2}(1-F_k^2) + \frac{\lambda}{2}F_m\right]s_k^+\right\} + \frac{1}{4}\sum_{k\rho}\left\{\sqrt{3}\,\lambda(G_{km}+F_kF_m)(s_k^+ - s_m^+) + \frac{3\lambda}{2}(2G_{km}+F_kF_m)(F_m s_m^+ + F_k s_k^+)\right\} \tag{26}$$

$$\hat{H}_3 = \frac{1}{4}\sum_{k\rho}\left\{-\frac{1}{2} - \frac{\sqrt{3}\,\lambda}{2}(F_m - F_k) - \frac{3\lambda}{2}(G_{km}+F_kF_m)\right\} \tag{27}$$

Here the summation over k runs over all triangular lattice sites, while the summation over ρ is over the three directed nearest-neighbour vectors that point from A to B, B to C, and C to A as required by the explicit bond directionality in the Hamiltonian given by Eq. (24), and the index $m \equiv k + \rho$. Each fundamental configuration for a given LSUBm approximation is then *pattern-matched* to each of the total 35 terms in the above similarity-transformed Hamiltonian following the procedure outlined in Appendix A to generate the entire set of coupled CCM ket-state equations. The CCM ket-state equations may then be solved by the Newton–Raphson method for nonlinear equations. Specifically, we start from the point $\lambda = 0$, at which we know the exact solution where all the correlation coefficients are zero. We then use this known solution as an initial input in solving the CCM equations for a slightly increased nonzero anisotropy λ. This procedure is carried out recursively to obtain the numerical results reported below.

D. Results

1. Ground-State Energy. In Fig. 6 we show the ground-state energy per spin E_g/N as a function of the anisotropy parameter λ for various LSUBm approximations. The corresponding values at the isotropic Heisenberg point are also tabulated in Table II. The highest-order calculation, LSUB6, which consists of 758 independent fundamental correlation coefficients, yields $E_g/N = -0.54290$. This value should be compared with the value -0.5445 extrapolated from finite-cluster diagonalisations of up to 36-spin clusters,[18] and the value -0.5431 ± 0.0001 from a recent QMC simulation.[46]

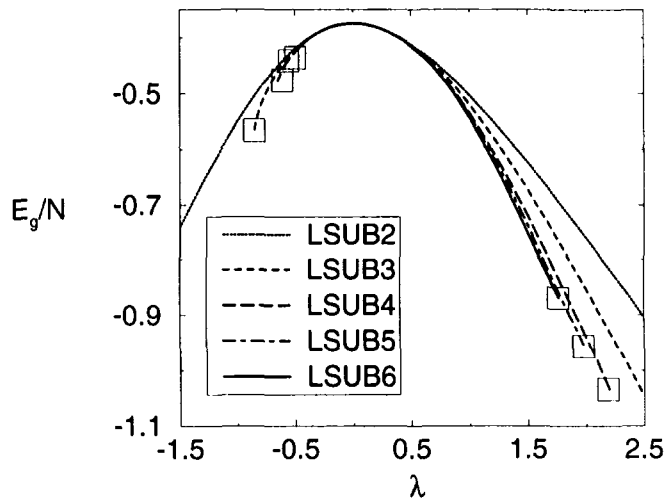

Fig. 6. Results for the CCM ground-state energy for the triangular HAF. LSUBm critical points λ_{c_1} and λ_{c_2} are indicated by the boxes.

As in Sec. 3D, we plot the LSUBm energies against $1/m^2$ and extrapolate these in the limit $m \to \infty$. We obtain an extrapolated value for the ground-state energy per spin of -0.5505 which is in good agreement with the series expansion calculations of Singh and Huse[15] who obtained a value for the ground-state energy per spin of -0.551. Compared with the corresponding classical value of -0.375, it is safe to say that the LSUB6 CCM calculation captures at least 99% of the quantum corrections.

To make further contact with the highest-order series expansion known to date,[15] we have computed the perturbative solution of E_g/N in terms of the anisotropy parameter λ. In Table III we tabulate the expansion coefficients from the LSUB6 approximation, together with the corresponding results from exact series expansions.[15] We note that the LSUB6 approximation reproduces the exact series expansion up to the 6th order. This result lends further strong support to the conjecture that the LSUBm approximation reproduces the *exact* series expansion to the same mth order.[48] Moreover, the fact that the corresponding values of several of the higher-order expansion coefficients from both the CCM LSUB6 perturbative solution and the exact series expansion remain close to each other shows that the exponential parametrization of the CCM with the inclusion of multi-spin correlations up to certain order also captures the dominant contributions to correlations of a few higher orders in the series expansions.

Table III. Expansion Coefficients in Powers of λ up to the 15th Order for the Ground-State Energy per Spin, E_g/N, and the Sublattice Magnetization for the Anisotropic Spin-1/2 Triangular-Lattice HAF Obtained from the CCM Equations in the LSUB6 Approximation[a]

Order	LSUB6: E_g/N	Exact: E_g/N	LSUB6: M^+	Exact: M^+
0	−0.3750000	−0.3750000	1	1
1	0.0000000	0.0000000	0	0
2	−0.1687500	−0.1687500	−0.27	−0.27
3	0.0337500	0.0337500	0.108	0.108
4	−0.0443371	−0.0443371	−0.2726916	−0.2726916
5	0.0204259	0.0204259	0.1717951	0.1717951
6	−0.0283291	−0.0283291	−0.3315263	−0.3315263
7	0.0311703	0.0315349	0.4060277	0.4110737
8	−0.0357291	−0.0476598	−0.5331858	−0.7382203
9	0.0541263	0.0685087	0.8894023	1.1781303
10	−0.0771681	−0.1025446	−1.3927395	−2.0109889
11	0.1294578	0.1565522	2.4179612	3.4012839
12	−0.1848858	?	−4.0426184	?
13	0.2857225	?	6.8086538	?
14	−0.4463496	?	−11.488761	?
15	0.7021061	?	19.388053	?

[a] The highest-order known exact series expansions up to the 11th order obtained by Singh and Huse[15] are also included for comparison.

As already displayed in Fig. 6, the LSUBm ground-state energy curve for $m \geqslant 3$ terminates at lower and upper critical values of the anisotropy, λ_{c_1} and λ_{c_2} respectively, beyond which no physical solution of the CCM ket-state equations exists. We have also tabulated λ_{c_1} and λ_{c_2} for various LSUBm approximations in Table II. Although the CCM based on the model state given in Eq. (A1) of Appendix A with the three-sublattice magnetic ordering is bound to break down in the region of the anisotropy parameter space where the true ground-state wavefunction possesses a different symmetry from that of the model state, it has been strongly argued[23, 26] that the terminating points may correspond to the critical points of a phase transition. Again the derivatives of the ground-state energy with respect to the anisotropy parameter may be analytically determined, and these derivatives of second and higher orders are found to diverge at the corresponding terminating anisotropy parameters λ_{c_1} and λ_{c_2}. Note that the lower terminating point λ_{c_1} clearly converges to a value of about -0.5, as argued by Singh and Huse.[15] However, the upper terminating point λ_{c_2}, as tabulated in Table II, remains considerably larger than the value of unity which was obtained via Padé analysis of the series

expansion by Singh and Huse.[15] Higher orders of approximation are needed to clarify this disagreement, though it is possible that the upper terminating point is highly singular and so convergence may be very slow. The detailed behaviour of the sublattice magnetization near λ_{c_2} is particularly suggestive with regard to this point, as discussed below. Also, further work is necessary in order to determine the singularity exponents of the ground-state energy at the two critical points.

2. Sublattice Magnetization. Once the ket- and bra-state correlation coefficients are known it is possible to evaluate the sublattice magnetization, $M^+ \equiv -2\langle s^z \rangle$, which is similarly defined by Eq. (21) except that the subscript i now covers all N_0 sites on the sublattice A, one of the three sublattices. In Table II we also tabulate the sublattice magnetization at the Heisenberg point for the various LSUBm approximations. The highest-order LSUB6 approximation gives give rise to a value of 0.6561. The extrapolated LSUBm value for the sublattice magnetization is 0.51, which now brings our results fully into line with those from the most careful analysis[18] to date of those from finite-size diagonalisation results and the second-order spin-wave calculations. We tend to believe that the corresponding result of $M^+ \approx 0.60$ from the fixed-node GFMC simulation[46] is likely to be too high, probably because the trial wavefunction on which it is based contains only two-and three-spin correlations.

The divergence in $\langle s^z \rangle$ seen in Fig. 7 near the critical points is a natural consequence of the approximate nature of the calculation. As we

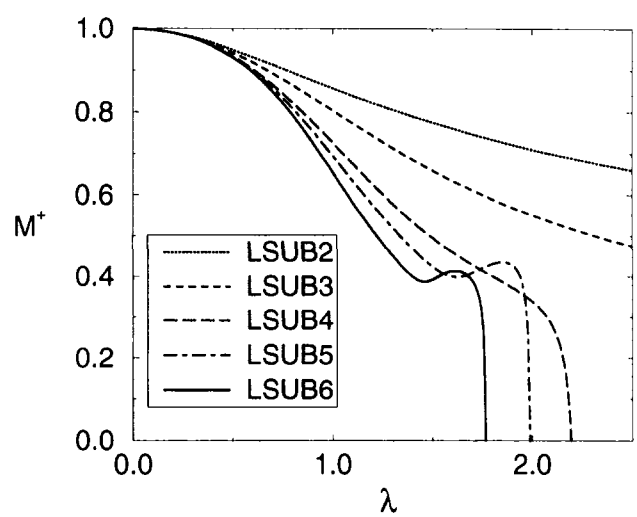

Fig. 7. Results for the CCM ground-state sublattice magnetization for the triangular HAF.

approach a critical point for a given LSUBm approximation, one of the CCM correlation coefficients x_r becomes very large. The contribution to $\langle s^z \rangle$ from this coefficient also becomes very large and so the sublattice magnetization diverges. The puzzling "upturn" of M^+ observed for the LSUB5 and the LSUB6 approximations near their respective upper critical points λ_{c_2} remains elusive to us at the present, although this behaviour is undoubtably correlated with the slow and erratic convergence of this antiferromagnetic critical point.

Again to make comparisons with the highest-order series expansion results, we perform a series expansion of the sublattice magnetization for a given LSUBm order of approximation, and results for LSUB6 are shown in Table III. We may also perform an Euler transformation and then re-sum these series, exactly as has been performed by Singh and Huse[15] using the exact series which is known to 11th order. We use exactly the same form of the Euler transform as these authors in order to compare their results with those of our CCM LSUBm calculations. The results are shown in Fig. 8, where the sublattice magnetization is plotted against $r^{-0.5}$ (r is the series expansion order). We can see that the LSUB6 series expansion results are converged up to approximately $r^{-0.5} \approx 0.3$, (i.e., up to order $r \approx 11$), and also that each LSUBm plot tends to the results obtained directly via direct evaluation of the CCM equations in the limit $r^{-0.5} \to 0$.

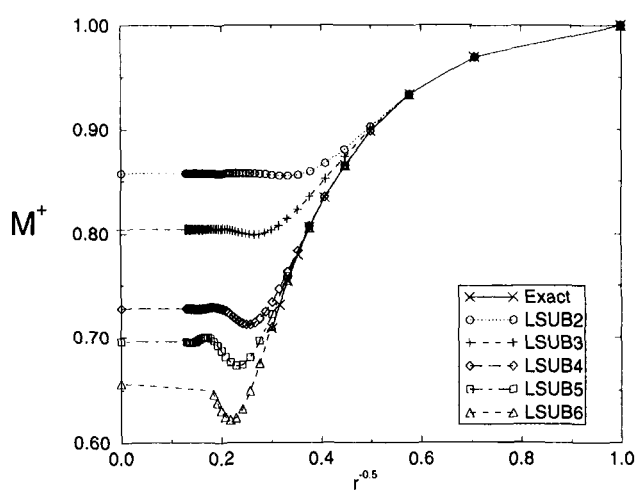

Fig. 8. The resummed series expansions of the sublattice magnetization plotted against $r^{-0.5}$ where r is the series order. The Euler transform was used with a value of $a = 1/3$, and the resulting series resummed. The CCM LSUBm resummed values for the sublattice magnetization converge to the analytical results shown in Table II as $r^{-0.5} \to 0$, and the exact series of Singh and Huse[15] is also shown.

However, we also see that if only a limited order of series terms are used—say fewer than about fifteen terms—then it is very easy to extrapolate to an incorrect LSUBm value, for the higher values of m, due to the "oscillation" which develops in the re-summed value of the sublattice magnetization as m increases. This presents the possibility that the re-summed exact series expansion results of Singh and Huse (also plotted in Fig. 8) were obtained at too low an order to observe this oscillation, which we believe might persist in the exact series limit, thus producing an incorrect extrapolation of the sublattice magnetization. Hence, from these results, and that of our extrapolated LSUBm results, we believe that the ground state of the triangular lattice HAF does indeed possess Néel-like long-range order.

In summary, compared with earlier applications of the CCM on the triangular HAF which have already revealed interesting oscillatory behaviour in long-ranged two-spin correlations,[33] the present high-order CCM calculations (with a systematic inclusion of multi-spin correlations on up to six contiguous lattice sites) have now obtained results for the ground-state energy and sublattice magnetization that are fully competitive with those obtained from other methods, and which are among the best available. Further detailed analysis of the large number of ket-state coefficients already obtained for the LSUB6 approximation, in order to achieve a better understanding of the nodal surface of the ground-state wavefunction, may provide a more microscopic justification of, and an extension to, the above-mentioned variational wavefunction. This may in turn lead to a better trial wavefunction for QMC simulations.

V. CONCLUSIONS AND OUTLOOK

In conclusion to this article, we restate our results which indicate that both the square-lattice and triangular-lattice HAFs contain Néel-like long-range order, and we also discuss our conjecture concerning previous series expansion calculations for the triangular-lattice HAF. We also briefly discuss the extension of our high-order calculations to further orders of approximation, and consider other systems to which the new formalism may be applied.

The success of our new formalism has meant that we are now able to attain much higher orders of approximation than ever before. For example, for the square-lattice HAF we have solved the LSUB8 approximation which contains over an order of magnitude more fundamental configurations than the previous best of LSUB6. These increases in the order of approximation have also resulted in increased accuracy of the ground-state energy and sublattice magnetization, even for the "raw" LSUBm results. A naive extrapolation of the sequence of LSUBm results yields values for

the sublattice magnetization of the quantum systems which contain 62% and 51% of the classical ordering for the square and triangular lattices respectively. Hence our CCM results are now fully consistent with the known behaviour of these models from the best of other approximate techniques.

We also make a conjecture concerning previous series expansion calculations for the triangular-lattice HAF. We have performed series expansion calculations of the ground-state energy and sublattice magnetization, and shown that our LSUBm results perfectly reproduce up to mth-order coefficients compared to those of the exact series expansions. Furthermore, for the triangular lattice HAF we find that the exact coefficients for orders greater than m are closely followed by the CCM coefficients. We performed an Euler transform and then re-summed the series, and observed that there is a characteristic oscillation about the result obtained via direct evaluation of the CCM equations in the re-summed value of the sublattice magnetization, plotted against $r^{-0.5}$ where r is the series expansion order. We believe that this oscillation might persist in the exact solution, and that if this is the case then previous exact series expansion calculations have not detected this oscillation because one needs to go to at least 15th order in the series before it becomes apparent. Thus, in this case, any extrapolation using a series of less than (approximately) 15th order would yield a much lower value for the sublattice magnetization than the true value.

The present results would be further clarified by the inclusion of even higher orders of approximation, and one possible way of achieving this might be to obtain and solve the CCM equations in *parallel*. We believe that the CCM is well suited to parallelisation as each CCM equation could be implemented on a separate processor.

We have already mentioned that our results using the new CCM formalism are now fully competitive with QMC and other results, and we have seen that our approach is easily generalisable to other systems. Possible future systems to which we may apply the new formalism include the valence-bond solids,[31, 36] systems with higher spin,[28, 29] and models with electronic degrees of freedom such as the Hubbard model.[51] The nature of the ground states of new and interesting materials or spin models might be quickly and easily investigated by specifying the Hamiltonian, lattice and spin number, and development of the code might therefore lead to a powerful test-bench for various new ideas. The future also holds the possibility of very high-order calculations, which will increase our knowledge both of these systems and also of the CCM. With the inclusion of very high orders of approximation it is also hoped that the asymptotic nature of the CCM ground-state energies, sublattice magnetizations and phase

transitions will become clear. In conclusion, we believe that the application of the CCM to the lattice spin systems is yielding excellent and interesting results, though there are still many avenues of fruitful and challenging research to be investigated.

APPENDIX A: COMPUTATIONAL ASPECTS OF THE CCM FOR SPIN-LATTICE MODELS

a. Ket-State CCM Equations

In this Appendix, a new way to implement the CCM formalism is presented which lends itself readily to high-order calculations. The computational aspects involved in the implementation of this new formalism are also described. The description here is kept as general as possible, and the model-specific details are discussed in the text of Secs. 3 and 4.

To make our assumptions clear, we restrict ourselves to spin-$\frac{1}{2}$ quantum antiferromagnets in the regimes where the corresponding classical limit is described by a generalized Néel-like ordering, i.e., where all spins on each sublattice are separately aligned in the coordinates of a global quantisation axis. However, it is a simple task (see Secs. 3 and 4 for details) to introduce a different local quantisation axis on each sublattice by a suitable spin-rotation transformation, such that the above Néel-like state becomes a fully aligned ("ferromagnetic") configuration in the local spin coordinates. This "ferromagnetic" state, $|\Phi\rangle$, is chosen as the uncorrelated CCM model state, where, in the local axes, all spins point along the respective negative z-axis,

$$|\Phi\rangle = \bigotimes_{i=1}^{N} |\downarrow\rangle_i; \text{ in the local quantization axes} \tag{A1}$$

The correlation operator S is then decomposed wholly in terms of sums of products of single spin-raising operators, $s_k^+ \equiv s_k^x + is_k^y$, again defined with respect to the local quantisation axes,

$$S = [i_1]\, s_{i_1}^+ + [i_1 i_2]\, s_{i_1}^+ s_{i_2}^+ + \cdots \tag{A2}$$

where $[i_1]$, $[i_1 i_2]$ and so on stand for the corresponding (symmetric) spin-correlation coefficients (recall $\{s_I\}$ in Sec. 2A) specified by the sets of site indices, $\{i_1\}$, $\{i_1, i_2\}$ and so on, on the regular lattices under consideration. Implicit summations over repeated indices are also assumed. According to

Eq. (7), the spin-correlation coefficients in Eq. (A2) are to be determined by a set of CCM nonlinear equations:

$$0 = \langle \Phi | s_{j_1}^- s_{j_2}^- \cdots s_{j_M}^- \mathrm{e}^{-S} H \mathrm{e}^{S} | \Phi \rangle \tag{A3}$$

where $s_{j_1}^- s_{j_2}^- \cdots s_{j_M}^-$ is the Hermitian conjugate of the corresponding multi-spin correlation string $s_{j_1}^+ s_{j_2}^+ \cdots s_{j_M}^+$.

In practice we clearly need an approximation scheme to truncate the expansion of S in Eq. (A2) to some finite or infinite subset of the full set of multi-spin configurations $\{I\}$. The three most commonly used truncation methods up till now are: (1) the SUBn scheme, in which all correlations involving only n or fewer spins are retained, however far separated on the lattice; (2) the simpler SUBn-m sub-approximation, where only SUBn correlations spanning a range of no more than m adjacent lattice sites are retained; and (3) the systematic local LSUBm scheme, which includes all multi-spin correlations over all possible distinct locales on the lattice defined by m or fewer contiguous sites. We note that only the last approximation scheme is adopted throughout this article.

The first step in the practical implementation of the LSUBm CCM is to enumerate all of the distinct multi-spin configurations or correlated clusters, which we shall henceforth call *fundamental* configurations, $\{i_1, i_2, ..., i_n\}$ with $n \leqslant m$, retained in the LSUBm approximation. It should be noted that the multi-spin configurations that are related by Hamiltonian symmetries, translational, rotational and reflectional alike, are counted as one single distinct configuration. Such a correlated cluster can be either a connected cluster of size m (also called a "lattice animal" or "polyomino") or a subset of it (connected or disconnected). Although the asymptotic behaviour of the number of lattice animals on a regular lattice remains an open combinatorial question, efficient algorithms for enumerating lattice animals up to sizes of about 20 have been developed in various fields including percolation and cell growth problems.[52]

The second step in our modular implementation, namely, generating the corresponding set of CCM equations, is what we will focus on in the remainder of this Appendix. Equation (A3) reveals that there are essentially two computational aspects involved in obtaining all possible non-zero contributions to its right-hand side. The first is to calculate the similarity-transformed Hamiltonian which then acts on the model state, and the second is to select terms of the similarity-transformed Hamiltonian that match exactly the string of spin-lowering operators represented by the set of site indices $\{j_1, j_2, ..., j_M\}$. The first aspect is intrinsically related to the noncommutative nature of quantum spin operators, and the second to the

geometric considerations of the lattice on which the Hamiltonian is defined. We address these two aspects in more detail below.

The computation of the similarity-transformed Hamiltonian, $\hat{H} \equiv e^{-S} H e^{S}$, which acts on the model state $|\Phi\rangle$ can be performed straightforwardly by making use of the relations $s^- |\Phi\rangle = 0$ and $s^z |\Phi\rangle = -\frac{1}{2} |\Phi\rangle$. The goal here is to completely eliminate s^z and s^-, and thus retain the creation operators only, by utilising the commutation relations of the spin operators, namely, $[s^z, s^\pm] = \pm s^\pm$ and $[s^-, s^+] = -2s^z$. This greatly simplifies the matching problem in-generating the CCM equations as discussed below. To this end, we note that the similarity-transformed single-spin operators can be expressed as:

$$\hat{s}_k^+ = s_k^+, \quad \hat{s}_k^z = s_k^z + F_k s_k^+, \quad \hat{s}_k^- = s_k^- - 2F_k s_k^z - (F_k)^2 s_k^+ \tag{A4}$$

where $F_k \equiv \sum_l l[k i_1 \cdots i_{l-1}]\, s_{i_1}^+ \cdots s_{i_{l-1}}^+$. Furthermore, the commutation relations between the spin operators and the F_k operators can also be written in the following compact forms,

$$\begin{aligned} [s_k^z, F_m] &= G_{km} s_k^+, & [s_k^-, F_m] &= -2G_{km} s_k^z \\ [s_k^z, (F_m)^2] &= 2F_m G_{km} s_k^+, & [s_k^-, (F_m)^2] &= -2(G_{km})^2 s_k^+ - 4F_m G_{km} s_k^z \end{aligned} \tag{A5}$$

where $G_{km} \equiv \sum_l l(l-1)[kmi_1 \cdots i_{l-2}]\, s_{i_1}^+ \cdots s_{i_{l-2}}^+$. Unlike in previous equations, repeated indices in Eqs. (A4) and (A5) *do not* imply summations. Clearly both F and G operators contain creation operators only. Consider then a typical two-spin interaction term, $s_k^- s_m^-$, for example, as contained in most spin-lattice Hamiltonians (see Secs. 3 and 4 for a full description of the quantum spin Hamiltonians actually studied in this article). It is easy to prove the following relation:

$$\begin{aligned} \hat{s}_k^- \hat{s}_m^- |\Phi\rangle = &\left(2(G_{km})^2 s_k^+ s_m^+ + 4F_k F_m G_{km} s_k^+ s_m^+ + (F_k)^2 (F_m)^2 s_k^+ s_m^+\right) |\Phi\rangle \\ &- \left(2G_{km} F_m s_m^+ + F_k (F_m)^2 s_m^+ + (F_k)^2 F_m s_k^+ + 2G_{km} F_k s_k^+\right) |\Phi\rangle \\ &+ (G_{km} + F_k F_m) |\Phi\rangle \end{aligned} \tag{A6}$$

In Eq. (A6), the resulting terms from $\hat{s}_k^- \hat{s}_m^-$ are classified into three categories as explicitly containing both s_k^+ and s_m^+, either s_k^+ or s_m^+, and neither s_k^+ nor s_m^+, respectively. The reason for such a classification becomes clear when we consider the second aspect, namely, generating the CCM equations. Thus, the first case is the simplest of all three to deal with, since the site indices of all terms in the case, including both k and m,

are completely fixed up to permutations by the *target* set $\{j_1, j_2, ..., j_M\}$ according to Eq. (A3). Although, unlike in the first case, only one of k and m in the second case must lie within the set $\{j_1, j_2, ..., j_M\}$, the search for k or m in the matching problem can be easily performed once m or k is fixed. This comes about since the two-spin interactions with which we mostly deal are usually short-ranged. Typical examples are the nearest-neighbour interactions where k and m are simply the nearest neighbours as in the two models considered in this article. By contrast, neither index k nor index m in the last case must belong to the set $\{j_1, j_2, ..., j_M\}$. Nonetheless, for the LSUBm approximation scheme used here, both k and m must lie within a *finite* set of indices for which $\{j_1, j_2, ..., j_M\}$ is a subset.

To be more specific, let us consider the term in Eq. (A6), $F_k F_m$, which can be written explicitly as:

$$F_k F_m = \sum_{l_1} \sum_{l_2} (l_1+1)(l_2+1)[ki_1 \cdots i_{l_1}][mn_1 \cdots n_{l_2}]\, s^+_{i_1} \cdots s^+_{i_{l_1}} s^+_{n_1} \cdots s^+_{n_{l_2}} \tag{A7}$$

where summation over repeated indices is implicitly assumed. Therefore, generating the part of the CCM equations due to this particular term $F_k F_m$ amounts to determining all possible non-zero contributions to $\langle \Phi | s^-_{j_1} \cdots s^-_{j_M} F_k F_m | \Phi \rangle$ according to Eq. (A7). This is achieved by partitioning the target set $\{j_1, j_2, ..., j_M\}$ into two subsets $\{i_1 \cdots i_{l_1}\}$ and $\{n_1 \cdots n_{l_2}\}$ with $l_1 + l_2 = M$, followed by a search for the appropriate k and m in a *nearby* region that includes $\{i_1 \cdots i_{l_1}\}$ and $\{n_1 \cdots n_{l_2}\}$ respectively, such that both correlation coefficients $[ki_1 \cdots i_{l_1}]$ and $[mn_1 \cdots n_{l_2}]$ are contained within the (symmetry-related) set of fundamental configurations retained by a given LSUBm approximation. Unlike earlier work[22, 23, 26] where the maximum number of fundamental configurations was limited to 100 or so, the present approach based on partition completely eliminates the costly procedure implemented previously for avoiding double occupancies of spin-$\frac{1}{2}$ objects, and thus reduces the CPU usage a great deal. This optimal implementation becomes possible because all of the terms (e.g., $F_k F_m$) in the similarity-transformed Hamiltonian ($\hat{H}$) and, more importantly, their explicit structures are completely specified by the *seemingly tedious* reformulation of $\hat{H}$ in terms of F_k, F_m, and G_{km} operators. The CCM ket-state equations so obtained can then be solved by the standard Newton–Raphson method.

b. Bra-State CCM Equations

According to Eq. (6) of Sec. 2, it is necessary to obtain both the ket-state correlation coefficients $\{s_I\}$ and the bra-state correlation coefficients

$\{\tilde{s}_I\}$ in order to compute a general ground-state physical quantity such as the sublattice magnetization. The task of generating the bra-state CCM equations (see Eq. (8)) turns out to be simple. Firstly, note that this set of coupled equations is linear in $\{\tilde{s}_I\}$, as is evident in Eq. (8); secondly, a simple equality, $\delta^2\bar{H}/\delta\tilde{s}_I\,\delta s_I = \delta^2\bar{H}/\delta s_I\,\delta\tilde{s}_I$, demonstrates that the bra-state equations can be readily generated from the already obtained CCM ket-state equations by appropriate differentiations.

Similarly, in the context of spin-$\frac{1}{2}$ quantum antiferromagnets, the $\tilde{S}$ operator is in general decomposed entirely in terms of annihilation operators which are again defined with respect to local quantisation axes:

$$\tilde{S} = 1 + [\widetilde{i_1}]\, s_{i_1}^- + [\widetilde{i_1 i_2}]\, s_{i_1}^- s_{i_2}^- + \cdots \tag{A8}$$

where $[\widetilde{i_1}]$, $[\widetilde{i_1 i_2}]$ and so on denote the corresponding bra-state spin-correlation coefficients specified by the sets of site indices $\{i_1\}$, $\{i_1, i_2\}$ and so on, which is the analogue of Eq. (A2). We note that we use the LSUBm approximation scheme here and that the coefficients $[i_1]$, $[i_1 i_2]$, and so on, and $[\widetilde{i_1}]$, $[\widetilde{i_1 i_2}]$, and so on, may be mapped onto sets $\{\mathscr{X}_r\}$ and $\{\tilde{\mathscr{X}}_r\}$ respectively, where r labels the *independent* or fundamental configurations: i.e., only those that are inequivalent under the lattice symmetries (namely, translations, rotations, and reflections) of the Hamiltonian and under permutations of the indices. The sets $\{\mathscr{X}_r\}$ and $\{\tilde{\mathscr{X}}_r\}$ are thus defined to count the independent correlation coefficients associated with each fundamental configuration once and once only. Generally speaking there will be $Nv_r(n_r)!$ equivalent configurations on the lattice associated with each fundamental configuration, where n_r is the number of sites in the rth configuration and $(n_r)!$ is the combinatoric factor associated with permutations of the n_r indices, the factor N arises from the translations, and the factor v_r is the replication factor of the rth configuration associated with the point symmetry group (or sub-group) of transformations on the lattice which preserve the Hamiltonian. In particular, we need only to consider one of the $Nv_r(n_r)!$ equivalent sets of equations (A3) associated with each independent coefficient $\mathscr{X}_r$. It is furthermore found very useful to introduce the notation that $x_r \equiv \mathscr{X}_r$ and $\tilde{x}_r \equiv (n_r!)\, v_r \tilde{\mathscr{X}}_r$ where r is the index of the rth fundamental configuration.

Now let $\delta\bar{H}/\delta\tilde{x}_r = P_r(x_1, x_2, ..., \lambda) = 0$ denote the rth ket-state CCM equation, which is given in terms of the ket-state correlation coefficients and λ, which stands for other parameters included in the Hamiltonian such as anisotropy, for example. Consequently $\bar{H}$ may now be written in terms of $P_r(x_1, x_2, ..., \lambda)$ and the bra-state correlation coefficients, $\{\tilde{x}_r\}$ as:

$$\bar{H} = P_0(x_1, x_2, ..., \lambda) + \sum_{r=1}^{N_F} \tilde{x}_r P_r(x_1, x_2, ..., \lambda) \tag{A9}$$

where $P_0(x_1, x_2,..., \lambda)$ denotes the zeroth-order CCM term, i.e., the ground-state energy expression, and N_F is the number of fundamental configurations retained for a given LSUBm approximation level. Therefore, the sth bra-state equation may now be rewritten in terms of $\tilde{x}_r$ and $P_r(x_1, x_2,..., \lambda)$:

$$\frac{\partial P_0(x_1, x_2,..., \lambda)}{\partial x_s} + \sum_{r=1}^{N_F} \tilde{x}_r \frac{\partial P_r(x_1, x_2,..., \lambda)}{\partial x_s} = 0; \qquad s = 1, 2,..., N_F \qquad \text{(A10)}$$

These linear equations for the coefficients $\{\tilde{x}_r\}$ may now be solved by using a standard decomposition technique, such as the LU decomposition method, once the ket-state correlation coefficients $\{x_r\}$ are known.

We note that similar algorithms have also been successfully implemented to study the excitation spectra. This will be the subject of a future publication.[42]

ACKNOWLEDGMENTS

We thank J. B. Parkinson and N. R. Walet for their interesting and useful discussions. C. Zeng gratefully acknowledges support from NSF grant DMR-9419257 at Syracuse University, and R. F. Bishop gratefully acknowledges a grant from the Engineering and Physical Sciences Research Council (EPSRC) of Great Britain.

REFERENCES

1. F. Coester, *Nucl. Phys.* **7**:421 (1958); F. Coester and H. Kümmel, *ibid.* **17**:477 (1960).
2. J. Čížek, *J. Chem. Phys.* **45**:4256 (1966); *Adv. Chem. Phys.* **14**:35 (1969).
3. R. F. Bishop and K. H. Lührmann, *Phys. Rev. B* **17**:3757 (1978).
4. H. Kümmel, K. H. Lührmann, and J. G. Zabolitzky, *Phys Rep.* **36C**:1 (1978).
5. J. S. Arponen, *Ann. Phys. (N.Y.)* **151**:311 (1983).
6. R. F. Bishop and H. Kümmel, *Phys. Today* **40**(3):52 (1987).
7. J. S. Arponen, R. F. Bishop, and E. Pajanne, *Phys. Rev. A* **36**:2519 (1987); *ibid.* **36**:2539 (1987); in *Condensed Matter Theories*, P. Vashishta, R. K. Kalia, and R. F. Bishop, eds. (Plenum, New York, 1987), Vol. 2, p. 357.
8. R. J. Bartlett, *J. Phys. Chem.* **93**:1697 (1989).
9. R. F. Bishop, *Theor. Chim. Acta* **80**:95 (1991).
10. F. D. M. Haldane, *Phys. Lett.* **93A**:464 (1983); *Phys. Rev. Lett.* **50**:1153 (1983).
11. S. R. White and D. A. Huse, *Phys. Rev. B* **48**:3844 (1993).
12. V. Kalmeyer and R. B. Laughlin, *Phys. Rev. Lett.* **59**:2095 (1987); *Phys. Rev. B* **39**:11879 (1989).
13. C. Zeng and V. Elser, *Phys. Rev. B* **42**:8436 (1990).
14. J. T. Chalker and J. F. G. Eastmond, *Phys. Rev. B* **46**:14201 (1992).
15. R. R. P. Singh and D. A. Huse, *Phys. Rev. Lett.* **68**:1766 (1992).
16. S. Sachdev, *Phys. Rev. B* **45**:12377 (1992).
17. K. Yang, L. K. Warman, and S. M. Girvin, *Phys. Rev. Lett.* **70**:2641 (1993).

18. B. Bernu, C. Lhuillier, and L. Pierre, *Phys. Rev. Lett.* **69**:2590 (1992).
19. N. Elstner and A. P. Young, *Phys. Rev. B* **50**, 6871 (1994).
20. B. Bernu, P. Lecheminant, C. Lhuillier, and L. Pierre, *Phys. Scripta* **T49**:192 (1993); *Phys. Rev. B* **50**:10048 (1994).
21. R. Deutscher, H. V. Everts, S. Miyashita, and M. Wintel, *J. Phys. A: Math. Gen.* **23**:L1043 (1990); R. Deutscher and H. V. Everts, *Z. Phys. B: Condensed Matter* **93**:77 (1993).
22. M. Roger and J. H. Hetherington, *Phys. Rev. B* **41**:200 (1990).
23. R. F. Bishop, J. B. Parkinson, and Y. Xian, *Phys. Rev. B* **43**, 13782 (1991); *Theor. Chim. Acta* **80**:181 (1991); *Phys. Rev. B* **44**:9425 (1991); in *Recent Progress in Many-Body Theories*, T. L. Ainsworth, C. E. Campbell, B. E. Clements, and E. Krotscheck, eds. (Plenum, New York, 1992), Vol. 3, p. 117.
24. F. E. Harris, *Phys. Rev. B* **47**:7903 (1993).
25. F. Cornu, Th. Jolicoeur, and J. C. Le Guillou, *Phys. Rev. B* **49**:9548 (1994).
26. R. F. Bishop, R. G. Hale, and Y. Xian, *Phys. Rev. Lett.* **73**:3157 (1994).
27. R. F. Bishop, R. G. Hale, and Y. Xian, *Phys. Rev. B* **46**:880 (1992).
28. W. H. Wong, C. F. Lo, and Y. L. Wang, *Phys. Rev. B* **50**:6126 (1994).
29. R. F. Bishop, J. B. Parkinson, and Y. Xian, *J. Phys.: Condens. Matter* **5**:9169 (1993).
30. D. J. J. Farnell and J. B. Parkinson, *J. Phys.: Condens. Matter* **6**:5521 (1994).
31. Y. Xian, *J. Phys.: Condens Matter* **6**:5965 (1994).
32. R. Bursill, G. A. Gehring, D. J. J. Farnell, J. B. Parkinson, T. Xiang, and C. Zeng, *J. Phys.: Condens. Matter* **7**:8605 (1995).
33. C. Zeng, I. Staples, and R. F. Bishop, *J. Phys.: Condens. Matter* **7**:9021 (1995); *Phys. Rev. B* **53**:9168 (1996).
34. C. Zeng and R. F. Bishop, in *Coherent Approaches to Fluctuations*, M. Suzuki and N. Kawashima, eds. (World Scientific, Singapore, 1996), p. 296.
35. C. F. Lo, K. K. Pang, and Y. L. Wang, *J. Appl. Phys.* **70**:6080 (1991).
36. Y. Xian, in *Condensed Matter Theories*, M. Casas, M. de Llano, and A. Polls, eds. (Nova Science Publ., Commack, New York, 1995), Vol. 10, p. 541.
37. P. W. Anderson, *Phys. Rev.* **86**:694 (1952); T. Oguchi, *ibid.* **117**:117 (1960).
38. R. R. P. Singh, *Phys. Rev. B* **39**:9760 (1989); W. Zheng, J. Oitmaa, and C. J. Hamer, *ibid.* **44**:11869 (1991).
39. J. Carlson, *Phys. Rev. B* **40**:846 (1989); N. Trivedi and D. M. Ceperley, *ibid.* **41**:4552 (1990).
40. K. J. Runge, *Phys. Rev. B* **45**:12292 (1992); *ibid.* **45**:7229 (1992).
41. D. A. Huse and V. Elser, *Phys. Rev. Lett.* **60**:2531 (1988).
42. D. J. J. Farnell, C. Zeng, J. B. Parkinson, and R. F. Bishop, unpublished.
43. T. Barnes, D. Kotchan, and E. S. Swanson, *Phys. Rev. B* **39**:4357 (1989).
44. K. Kubo and T. Kishi, *Phys. Rev. Lett.* **61**:2585 (1988).
45. W. F. Lunnon, in *Graph Theory and Computing*, R. C. Read, ed. (Academic Press, New York, 1972), p. 87.
46. M. Boninsegni, *Phys. Rev. B* **52**:5304 (1995).
47. P. W. Leung and K. Runge, *Phys. Rev. B* **47**:5861 (1993).
48. R. F. Bishop, J. B. Parkinson, and Y. Xian, *J. Phys.: Condens. Matter* **4**:5783 (1992).
49. C. Zeng, D. J. J. Farnell, and R. F. Bishop, unpublished.
50. B. Flaming, *Practical Data Structures in C++*, (Coriolis Group Book, Wiley, New York, 1993), p. 281.
51. M. Roger and J. H. Hetherington, *Europhys. Lett.* **11**:255 (1990); C. F. Lo, E. Manousakis, and Y. L. Wang, *Phys. Lett. A* **156**:42 (1991); F. Petit and M. Roger, *Phys. Rev. B* **49**:3453 (1994); R. F. Bishop, Y. Xian, and C. Zeng, *Int. J. Quantum Chem.* **55**:181 (1995).
52. S. Mertens, *J. Stat. Phys.* **58**:1095 (1990).